A nonlinear model of thermoacoustic devices

Sergey Karpov and Andrea Prosperetti[a)]
Department of Mechanical Engineering, The Johns Hopkins University, Baltimore, Maryland 21218

(Received 22 October 2001; revised 21 June 2002; accepted 25 June 2002)

This paper presents a nonlinear, time-domain model of thermoacoustic devices based on cross-sectional averaged equations. Heat transfer perpendicular to the device axis—which lies at the core of thermoacoustic effects—is modeled in a novel and more realistic way. Heat conduction in the solid surfaces surrounding the fluid medium is included. Contrary to the previous versions of this model [Watanabe *et al.*, J. Acoust. Soc. Am. **102**, 3484–3496 (1997)], the present version does not require artificial damping and is numerically robust. The model performance is illustrated on several examples: a prime mover, an externally driven thermoacoustic refrigerator, and a combined prime mover/refrigerator system. © *2002 Acoustical Society of America.* [DOI: 10.1121/1.1501277]

PACS numbers: 43.35.Ud, 43.25.Gf, 84.60.Rb, 43.20.Ks [RR]

I. INTRODUCTION

The physical process at the heart of thermoacoustic prime movers and refrigerators is the exchange of energy between the working fluid and the solid structure in contact with it (see, e.g., Rott, 1980; Wheatley, 1986; Swift, 1988). While in a multidimensional description of these devices the modeling of this exchange process arises naturally through the solution of the balance equations for momentum and energy, in a quasi-one-dimensional description specific models are needed (see, e.g., Watanabe *et al.*, 1997; Mozurkewich, 1998a).

In our earlier work on one such quasi-one-dimensional description (Watanabe *et al.*, 1997; Yuan *et al.*, 1997), we have used relatively crude models inspired by a straightforward application of linear theory. We found that, while many features of the nonlinear behavior of thermoacoustic prime movers observed in experiment could be reproduced by the model, numerical difficulties remained that deprived the calculation of the degree of robustness necessary for a widespread acceptance of the formulation.

The primary purpose of the present paper is to present a better model for the description of the exchange of momentum and energy between the fluid and the solid. At a cost of a minimal increase in complexity, we achieve a greater physical realism, a much stronger degree of numerical stability, and we are able to dispense with the introduction of artificial numerical damping that was needed in our earlier model (Yuan *et al.*, 1997). A second purpose of the paper is to include heat transport by conduction in the stack and in the heat exchangers that was neglected in the earlier formulations.

As a result of these two extensions, we present a general time-domain, fully nonlinear model of thermoacoustic devices that is capable of predicting the response of such systems to cross-sectional area variations, stack position, fluid properties, and many other design variables. While the model is not exact due to the averaging over the cross section, in the frequency domain and for small amplitudes it reduces to the standard linear theory. In addition, it is able to describe nonlinear phenomena such as the finite-amplitude saturation of the thermoacoustic instability while, at the same time, remaining substantially simpler than a truly multidimensional model. We thus hope that our model can be useful in filling the current gap in the levels of description available for thermoacoustic systems.

In particular, only limited theoretical information exists on nonlinear phenomena in thermoacoustic devices. Examples of analytical studies include Bauwens (1996, 1998), who studied large-amplitude oscillations in the limit of a nearly uniform gas temperature over the cross section of a round tube, Gopinath *et al.* (1998), who investigated the steady-state temperature distribution in the stack by a second-order regular perturbation theory, and a recent one by the present authors where the time-dependent nonlinear saturation of the thermoacoustic instability was obtained by a method of multiple time scales carried to fourth order (Karpov and Prosperetti, 2000). Numerical work includes a paper by Cao *et al.* (1996), in which the heat exchange between the gas and zero-thickness stack plates in a thermoacoustic couple is calculated, and the papers by Worlikar and Knio (1996, 1999), Worlikar *et al.* (1998), and the thesis by Worlikar (1997), which focus on the two-dimensional modeling of flow and heat transfer in the stack region including the blockage effect of the stack; in these studies—unlike the present formulation—the rest of the system is modeled as a single-frequency acoustic wave. In a very recent paper Hamilton *et al.* (2002) present an interesting nonlinear model constructed on boundary-layer-like approximations.

Although understandable in view of the complexity of the problem, the paucity of papers devoted to nonlinear effects is unfortunate as ample experimental evidence exists as to their importance. The very fact that the thermoacoustic instability in a prime mover ultimately saturates at a finite pressure amplitude is an obvious consequence of nonlinearity.[1] More subtly, as pointed out by Worlikar *et al.* (1998), some of the differences between linear theory and experiment encountered by Atchley *et al.* (1990a) are to be attributed to nonlinearity already at drive ratios as low as

[a)]Also at Faculty of Applied Physics and Twente Institute of Mechanics, University of Twente, AE 7500 Enschede, The Netherlands, and Burgerscentrum, The Netherlands.

2%. Furthermore, it may be argued that the effective exploitation of thermoacoustic systems requires operation in the nonlinear regime. The strongly nonlinear resonators described by Ilinskii *et al.* (1998) are a particularly interesting possibility.

II. SIMPLIFIED MODELS OF THERMOACOUSTIC DEVICES

We begin by a summary of the simplified model of thermoacoustic devices used in our previous papers (Watanabe *et al.*, 1997; Yuan *et al.*, 1997).

The key simplification rests on the observation that, in most thermoacoustic devices, the dimensions of the system in the direction of the fluid particle displacement are much greater than those normal to it. This circumstance suggests the use of a quasi-one-dimensional model in which the conservation equations for mass, momentum, and energy are averaged over the cross section of the system. Details on the derivation can be found in Watanabe *et al.* (1997), and here we simply summarize the results.

The equation of continuity is

$$\frac{\partial \rho}{\partial t}+\frac{1}{S}\frac{\partial}{\partial x}(S\rho u)=0. \tag{1}$$

Here, x is the coordinate along the axis of the device (not necessarily rectilinear), $S(x)$ is the local cross-sectional area, and ρ and u are the gas density and axial velocity, respectively, averaged over the cross-sectional area. The momentum equation takes the form

$$\frac{\partial}{\partial t}(\rho u)+\frac{1}{S}\frac{\partial}{\partial x}(S\rho u^2)+\frac{\partial p}{\partial x}=-\ \rho\ \mathcal{D}(u), \tag{2}$$

where p is the cross-sectional average of the gas pressure and the term $\mathcal{D}(u)$ accounts for momentum exchange between the fluid and the surrounding solid surfaces and will be specified shortly. On the assumption of perfect-gas behavior, the energy equation is written in the form

$$\frac{\partial}{\partial t}\left(\frac{1}{\gamma-1}\ p+\frac{1}{2}\rho u^2\right)+\frac{1}{S}\frac{\partial}{\partial x}\left[uS\left(\frac{\gamma}{\gamma-1}\ p+\frac{1}{2}\rho u^2\right)\right]$$
$$=\rho c_p\left[\mathcal{H}(T_w-T)-\frac{dT_w}{dx}\mathcal{Q}\ u\right], \tag{3}$$

where γ is the ratio of the gas-specific heats, T the cross-sectional average of the gas temperature, and T_w the surface temperature of the solid surfaces in contact with the gas. The terms $\mathcal{H}$, $\mathcal{Q}$ are analogous to $\mathcal{D}$ and account for the exchange of energy between the fluid and the solid; these quantities are at the core of the present study and will be discussed in detail below [some comments on the form of the right-hand side of (3) are given in the Appendix]. It is further postulated that the perfect gas equation of state

$$p=\mathcal{R}\rho T, \tag{4}$$

where $\mathcal{R}$ is the universal gas constant divided by the gas molecular mass, is satisfied by the cross-sectional averages.

Closure of the model requires knowledge of the temperature distribution T_w along the axis of the device. In our earlier papers this quantity was taken as given and independent of time, but one can easily remove this restriction by once more using a cross-sectional average, this time over the solid material that constitutes the stack. Although it is not necessary to specify the geometrical structure of the stack, for ease of exposition we will think of it as constituted by a set of parallel plates. Area averaging is justified by the fact that the plates are usually thin; a similar remark would apply to pin stacks or other geometrical arrangements. In this way, one finds

$$\rho_s c_s\frac{\partial T_w}{\partial t}=\frac{1}{S_s}\frac{\partial}{\partial x}\left(k_s S_s\frac{\partial T_w}{\partial x}\right)$$
$$-\ \rho c_p\left[\mathcal{H}(T_w-T)-\frac{dT_w}{dx}\mathcal{Q}\ u\right], \tag{5}$$

where ρ_s, c_s, k_s, and S_s are the density, specific heat, thermal conductivity, and cross-sectional area of the plates, respectively. The heat exchangers are modeled in a similar way, except that their thermal conductivity is taken to be infinite so that their temperature is spatially uniform.[2] For the sake of simplicity, in the examples that follow we assume that the stack plates are in perfect thermal contact with the cold and hot heat exchangers.

Away from the stack region, one could use a similar formulation for the resonator tube walls, or one could couple the model equations with the conduction equations in the walls. In this study, for simplicity, we shall simply assume that the tube wall temperature is prescribed.

A variety of boundary conditions can be associated with the mathematical model described before depending on the situation that it is desired to model. For example, for the prime mover case with standing waves, it might be reasonable to assume that the end walls of the tube are rigid, so that the velocity vanishes

$$u=0 \quad \text{at } x=0, \quad x=L. \tag{6}$$

The momentum equation (2) then implies that

$$\frac{\partial p}{\partial x}=0 \quad \text{at } x=0, \quad x=L. \tag{7}$$

Equations (1) and (3) written at the endpoints ($x=0$, L) then give

$$\frac{\partial \rho}{\partial t}+\rho\frac{\partial u}{\partial x}=0, \tag{8}$$

$$\frac{\partial p}{\partial t}+\ \gamma p\frac{\partial u}{\partial x}=(\gamma-1)\ \rho c_p\ \mathcal{H}(T_w-T). \tag{9}$$

Upon eliminating $\partial u/\partial x$, one finds

$$\frac{\partial T}{\partial t}=\frac{\gamma-1}{\gamma}\frac{T}{p}\frac{\partial p}{\partial t}+\ \mathcal{H}(T_w-T). \tag{10}$$

This relation shows that a knowledge of p at the boundary completely specifies T. No additional boundary conditions are therefore necessary. Since the heat transfer term $\mathcal{H}$ is very small outside the stack region, this relation then essentially implies the adiabatic pressure-temperature relation of perfect gases.

In general, the relation (10) would result in a temperature jump from the T given by this relation to the end-wall temperature. This is a consequence of the neglect of axial conduction in the derivation of the energy equation (3). Axial conduction would introduce a term $\partial^2 T/\partial x^2$, important only near the end walls, the role of which would be to re-establish continuity of temperature by means of a thin boundary layer. The temperature in this layer would adjust itself so as to match the value given by (10). This is an essentially passive process with negligible effects on the temperature distribution elsewhere in the device and can therefore be disregarded. If desired, however, the expression for $\mathcal{H}$ can be adjusted to give a heat transfer coefficient at the tube ends.

For the case of standing waves forced by a piston, as in a refrigerator arrangement, one might consider two limit cases. The piston may be located at a velocity antinode, corresponding to a pressure node. In this case one may assume a vanishing pressure disturbance and an imposed fluid velocity at this location. Conversely, for a piston located at a pressure antinode, one may use an imposed pressure condition and a zero velocity condition.

These models can of course be refined. For example, more complicated end-wall impedances may be accounted for by prescribing, in place of (6), (7), a relation coupling pressure and velocity at $x=0, L$. The use of periodicity conditions at the tube ends would permit to model a toroidal traveling wave system, and so on.

III. THE EXCHANGE TERMS

It was shown in Watanabe *et al.* (1997) that, upon linearization, in the frequency domain the model (1) to (4) leads to the following eigenvalue equation for the pressure perturbation p':

$$\frac{1}{S}\frac{d}{dx}\left[\frac{Sc_A^2}{1+\hat{D}/(i\omega)}\frac{dp'}{dx}\right]+\omega^2 p' + \frac{\hat{H}}{i\omega}\left\{\frac{c_A^2}{S}\frac{d}{dx}\left[\frac{S}{1+\hat{D}/(i\omega)}\frac{dp'}{dx}\right]+\gamma\omega^2 p'\right\} + \frac{(\gamma-1)c_p}{1+\hat{D}/(i\omega)}\frac{dT_w}{dx}\hat{Q}\frac{dp'}{dx}=0, \tag{11}$$

where $c_A^2=\gamma\mathcal{R}T_w$ is the local adiabatic sound speed, and proportionality to $\exp(i\omega t)$ has been assumed. In deriving this equation we have set

$$\mathcal{D}(u)=\hat{D}(\omega)u, \quad \mathcal{H}(T_w-T)=\hat{H}(\omega)(T_w-T), \quad \mathcal{Q}u=\hat{Q}(\omega)u. \tag{12}$$

In the same paper it was also shown that the choices

$$\hat{D}(\omega)=i\omega\frac{f_V}{1-f_V}, \tag{13}$$

$$\hat{H}(\omega)=i\omega\frac{f_K}{1-f_K}, \quad \hat{Q}(\omega)=\frac{1}{1-\sigma}\left(\frac{f_V}{1-f_V}-\frac{\sigma f_K}{1-f_K}\right), \tag{14}$$

reduce (11) to the well-known linear formulation of Rott (1976, 1980; see also Swift, 1988). In (13) and (14) the quantities $f_{V,K}$ depend on the ratio of the diffusion lengths to the hydraulic diameter of the flow passage (Rott, 1980; Wheatley, 1986; Swift, 1988; Arnott *et al.*, 1991). The viscous and thermal diffusion lengths $\delta_{V,K}$ are given by

$$\delta_V=\sqrt{\frac{2\nu}{\omega}}, \quad \delta_K=\sqrt{\frac{2\alpha}{\omega}}=\frac{\delta_V}{\sqrt{\sigma}}, \tag{15}$$

respectively, with ν the kinematic viscosity, σ the Prandtl number, and $\alpha=\nu/\sigma$ the thermal diffusivity. We keep the Prandtl number constant, but we account for the dependence of ν and α on the local temperature and pressure.

For parallel plates with a spacing l, one has (Swift, 1988)

$$f=(1-i)\frac{\delta}{l}\tanh(1+i)\frac{l}{2\delta}, \tag{16}$$

with index V or K; graphs of $if/(1-f)$ for this case are given in Watanabe *et al.* (1997). For circular flow passages with radius r_0 (Rott, 1969)

$$f=\frac{2J_1((i-1)(r_0/\delta))}{(i-1)(r_0/\delta)\,J_0((i-1)(r_0/\delta))}, \tag{17}$$

where $J_{0,1}$ are Bessel functions.

Since a very well developed theory exists for the linear problem in the frequency domain, the value of the present simplified model consists of its ability to give information on nonlinear, time-domain processes for which no exact theory is available short of direct, multidimensional numerical simulations. In order to accomplish this goal, however, it is necessary to develop a suitable time-domain formulation for the transfer terms.

In our earlier work (Yuan *et al.*, 1997), our first attempt was to simply take[3]

$$\mathcal{D}(u)=D\left(1+\theta_D\frac{\partial}{\partial t}\right)u, \tag{18}$$

with D,θ_D constants determined in such a way that

$$D(1+i\omega_1\theta_D)=\hat{D}(\omega_1), \tag{19}$$

where ω_1 is the real part of the frequency of the fundamental mode of the system; similar forms were postulated for the other exchange terms. This choice was based on the fact that the fundamental mode at frequency ω_1 is usually the most important one, and it was therefore desirable to simulate it as precisely as possible. Unfortunately, as discussed in Yuan *et al.* (1997), this simple choice is inadequate as it causes many high-order modes of the system to become unphysically unstable, which causes difficulties in numerical work; an example was given in Fig. 1 of that paper.

In order to remedy the situation, an *ad hoc* damping contribution was artificially added to the term $\mathcal{H}$, which resulted in a spectrum with the desired stability features. While effective, this procedure is undesirable for two reasons, one practical and one of principle. On the practical side, the determination of the parameters of the new term requires the ability to calculate the eigenvalue spectrum of (a suitably

modified form of) Eq. (11), which is a nontrivial task. As a matter of principle, the new dissipative term appears suspicious due to its lack of a physical basis. These considerations led us to an attempt to improve the situation that we now describe.

IV. NEW FORM OF THE ENERGY AND MOMENTUM EXCHANGE TERMS

In attempting to tackle the problem mentioned in the previous section, we decided to follow the suggestion of Achard and Lespinard (1981), who were interested in finding a quasi-one-dimensional formulation for the time-dependent viscous flow of a fluid in a duct. While, with the assumption of fully developed flow, the problem is linear and can be solved by Laplace transform methods, they realized that no form for the drag term short of a time convolution can capture exactly the physics of the process. For this reason, they proposed an approximation in which the momentum transfer term was not given by a single constant, but was found by solving an ordinary differential equation in time.

The simplest form is

$$a_D \frac{d\mathcal{D}}{dt} + \mathcal{D} = b_D \left(1 + c_D \frac{d}{dt}\right) u, \tag{20}$$

with a_D, b_D, c_D three suitable real constants. If $a_D = 0$, this relation reduces to the earlier choice (18) but, in general, it contains one additional parameter that can be chosen so as to improve the representation of the fluid–solid momentum transfer. We proceed in a similar fashion for the other exchange terms as well

$$a_H \frac{d\mathcal{H}}{dt} + \mathcal{H} = b_H \left(1 + c_H \frac{d}{dt}\right) (T_w - T), \tag{21}$$

$$a_Q \frac{d\mathcal{Q}u}{dt} + \mathcal{Q}u = b_Q \left(1 + c_Q \frac{d}{dt}\right) u. \tag{22}$$

In the frequency domain, all these prescriptions reduce to (12) with $\hat{D}$, $\hat{H}$, $\hat{Q}$ replaced by

$$\tilde{D}(\omega) = b_D \frac{1 + i\omega c_D}{1 + i\omega a_D}, \tag{23}$$

etc. We are now at liberty to impose three conditions in order to determine the model parameters *a*, *b*, *c*. As in our earlier model, in view of the importance of the fundamental mode at frequency ω_1, we impose that

$$\tilde{D}(\omega_1) = b_D \frac{1 + i\omega_1 c_D}{1 + i\omega_1 a_D} = \hat{D}(\omega_1), \tag{24}$$

with $\hat{D}(\omega)$ given by (13); here, as before, ω_1 is the real part of the complex eigenfrequency $\hat{\omega}_1$ of the first mode. Satisfaction of this condition ensures that the eigenvalue of the first mode of Rott's theory is reproduced. Upon separating real and imaginary parts, we find two equations among the three real parameters a_D, b_D, c_D.

For the remaining condition there is considerable latitude. Physically, since the transverse dimensions of the flow passages in the stack are usually much smaller than the stack length, one can make the approximation of fully developed flow in the stack. If the physical properties of the fluid were constant, this approximation would have the effect of rendering the left-hand side of the exact conservation equations linear, which would permit one to consider each mode separately.[4] From this point of view, the best approach would be to choose the remaining constant so as to minimize the difference between the exact and approximate linear spectra. This objective can be achieved, but once more at the cost of solving the eigenvalue problem exactly.

Hence, we propose a simpler alternative. In a thermoacoustic prime mover, it is usually the first mode that is unstable. As its amplitude grows, it loses energy to the second and higher modes by nonlinear couplings. The second mode is excited the most and, since it is stable, it will represent the greatest energy sink for the system. The situation is similar in a thermoacoustic refrigerator, where the forcing typically energizes the fundamental mode the most with, again, the second mode providing the greatest energy loss (after the fundamental). These considerations suggest that an effective second condition for the determination of the last free constant in the exchange terms is to impose that the damping of the second mode be correctly described. We cannot use condition (24) for the second mode since the real and imaginary parts of the relation (24) give two equations, but only one free constant remains available. To choose the right condition we use as a guide an earlier result [Karpov and Prosperetti (1998), Eqs. (33), (34); Karpov and Prosperetti (2000), Eq. (5.4)] according to which the linear growth (or damping) rate of the generic *n*th mode can be approximated by

$$\begin{aligned} \mathrm{Im}\ \hat{\omega}_n = \frac{1}{2Vp_0^2\omega_n} \int_0^L dx\ S \Bigg[& \frac{c_A^2}{\omega_n} \mathrm{Re}\ \hat{D}(\omega_n) \left(\frac{dP_n}{dx}\right)^2 \\ & + \gamma\omega_n\ \mathrm{Re}\ \hat{H}(\omega_n) P_n (P_n - \mathcal{R}R_n T_w) \\ & + (\gamma - 1)\ \mathrm{Im}\ \hat{Q}(\omega_n) c_p \frac{dT_w}{dx} P_n \frac{dP_n}{dx} \Bigg]. \end{aligned} \tag{25}$$

This result shows that $\mathrm{Im}\ \hat{\omega}_n$ depends on $\mathrm{Re}\ \hat{D}(\omega_n)$, $\mathrm{Re}\ \hat{H}(\omega_n)$, and $\mathrm{Im}\ \hat{Q}(\omega_n)$, which suggests the following conditions:

$$\mathrm{Re}\ \hat{D}(\omega_2) = b_D\ \mathrm{Re} \frac{1 + i\omega_2 c_D}{1 + i\omega_2 a_D}, \tag{26}$$

$$\begin{aligned} \mathrm{Re}\ \hat{H}(\omega_2) &= b_H\ \mathrm{Re} \frac{1 + i\omega_2 c_H}{1 + i\omega_2 a_H}, \\ \mathrm{Im}\ \hat{Q}(\omega_2) &= b_Q\ \ \mathrm{Im} \frac{1 + i\omega_2 c_Q}{1 + i\omega_2 a_Q}. \end{aligned} \tag{27}$$

Here, ω_2 is the real part of the complex eigenfrequency of the second mode $\hat{\omega}_2$.[5]

In order to demonstrate the quality of the approximations thus obtained, in Figs. 1 and 2 we compare the ω-dependence of the functions $\tilde{D}$ and $\tilde{Q}$ given by (20), (22) with the expressions $\hat{D}$, $\hat{Q}$ given in (13), (14). The Prandtl number is $\sigma = 0.71$ and, at the frequency ω_1, $\delta_K/l = 0.34$. Since the expression for the operator $\mathcal{H}$ is similar to the expression for operator $\mathcal{D}$, we do not show it.

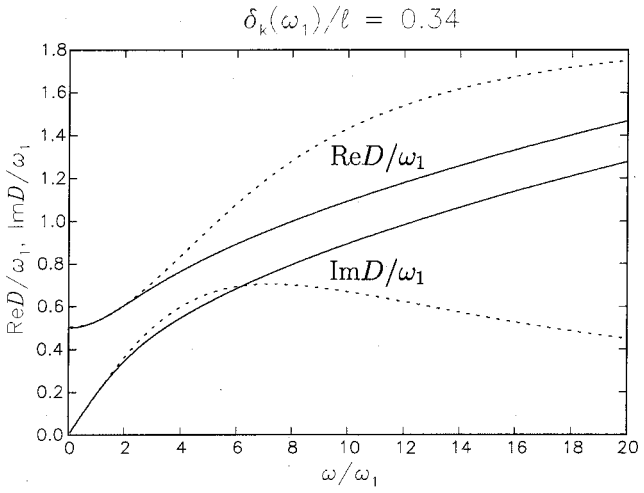

FIG. 1. Real and imaginary parts of the exact function $\hat{D}(\omega)$ defined in (13) (solid lines) compared with real and imaginary parts of the approximation for $\tilde{D}(\omega)$ given by (23) (dotted lines) for the ratio $\delta_K(\omega_1)/l=0.34$ and Prandtl number $\sigma=0.71$.

As formulated above, it would seem that the determination of the model requires the solution of the linear eigenvalue problem, at least for the determination of $\hat{\omega}_1$ and $\hat{\omega}_2$. Actually, this task can be considerably simplified as the real part of the eigenfrequencies is very well approximated by neglecting the exchange terms in the eigenvalue equation (11)

$$\frac{1}{S}\frac{d}{dx}\left(Sc_A^2\frac{dp'}{dx}\right)+\omega_1^2 p'=0. \tag{28}$$

A further simplification is obtained by using, for c_A, a value based on the average temperature of the resonator

$$T_e=\frac{1}{L}\int_0^L T_w\,\mathrm{d}x. \tag{29}$$

In particular, for a cylindrical tube closed at the two ends, one may take

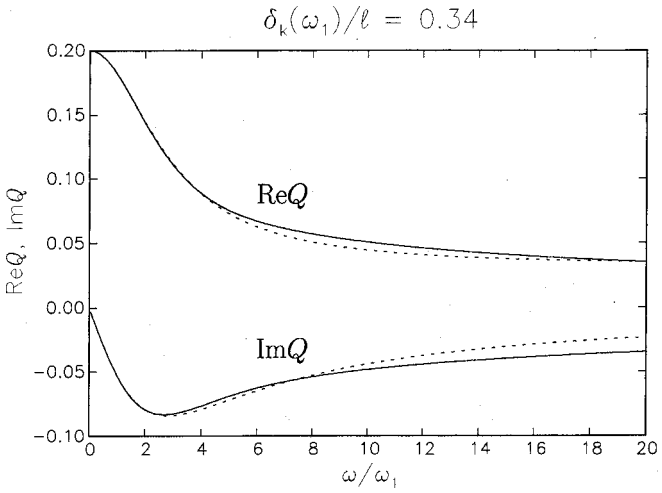

FIG. 2. Real and imaginary parts of the exact function $\hat{Q}(\omega)$ defined in (14) (solid lines) compared with real and imaginary parts of the approximation for $\tilde{Q}(\omega)$ given by the analog of (23) (dotted lines) for the ratio $\delta_K(\omega_1)/l=0.34$ and Prandtl number $\sigma=0.71$.

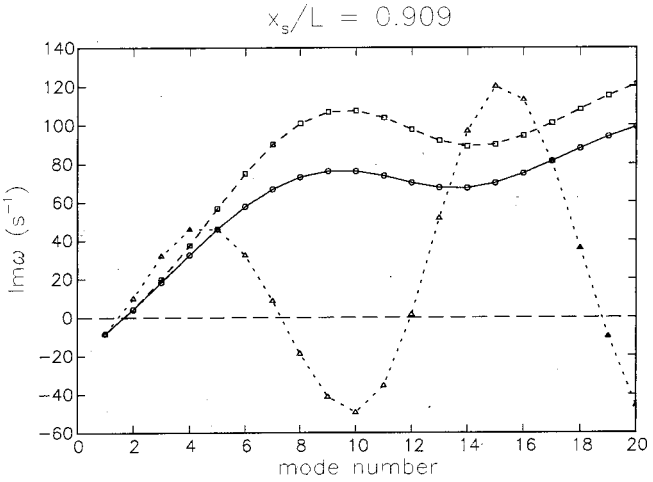

FIG. 3. Damping constant of the first 20 eigenmodes for the system and conditions described in Sec. IV; the stack is located at $x_s/L=0.909$. The circles are the results of Rott's linear theory. The squares and triangles correspond to the differential equation approximation (20)–(22) to the momentum and energy exchange terms and to the simple explicit form (19), respectively. The lines are only meant as guides to the eye.

$$\omega_1 \simeq \frac{\pi}{L}\sqrt{\gamma\mathcal{R}T_e},\quad \omega_2 \simeq 2\omega_1. \tag{30}$$

We found that usually this approximation for ω_1 is sufficient. Approximations are also available for tubes of nonuniform cross section (see, e.g., Rayleigh, 1896), although (30) may give an adequate approximation in many of these cases as well.

As examples of the effect of the previous approximations on the linear spectrum of the problem, Figs. 3, 4, and 5 show the damping constant of the first 20 eigenmodes as a function of the mode number for three different positions of the stack midpoint, $x_s/L=0.91,0.77,0.68$; instability corresponds to a negative value of the quantity shown. The circles connected by the solid line are the result of the standard linear theory (11). Note that in all the examples only the first

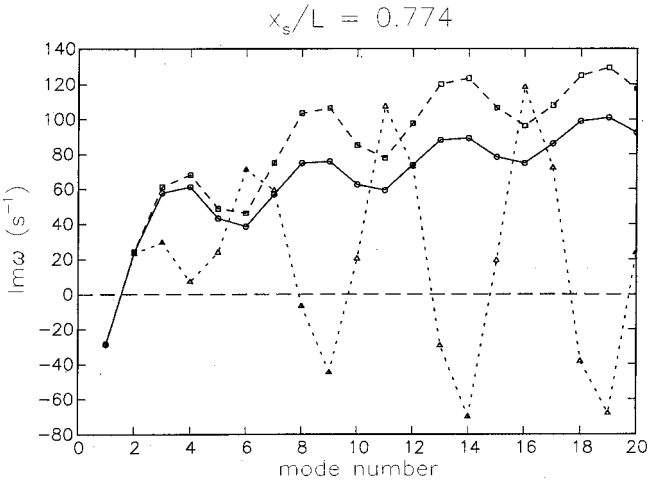

FIG. 4. Damping constant of the first 20 eigenmodes for the system and conditions described in Sec. IV; the stack is located at $x_s/L=0.774$. The circles are the results of Rott's linear theory. The squares and triangles correspond to the differential equation approximation (20)–(22) to the momentum and energy exchange terms and to the simple explicit form (19), respectively. The lines are only meant as guides to the eye.

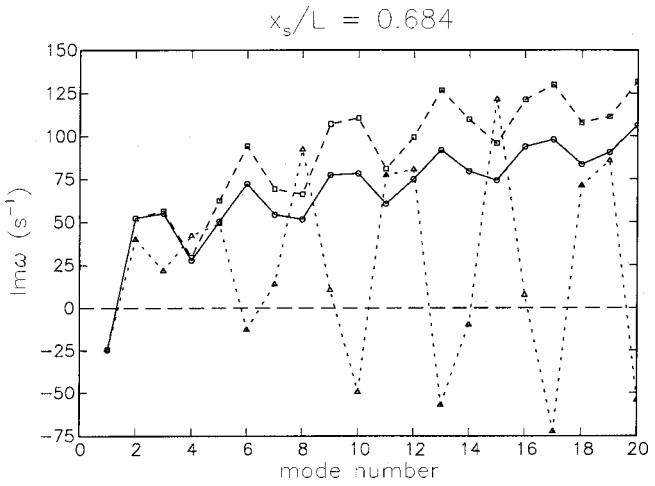

FIG. 5. Damping constant of the first 20 eigenmodes for the system and conditions described in Sec. IV; the stack is located at $x_s/L=0.684$. The circles are the results of Rott's linear theory. The squares and triangles correspond to the differential equation approximation (20)–(22) to the momentum and energy exchange terms and to the simple explicit form (19), respectively. The lines are only meant as guides to the eye.

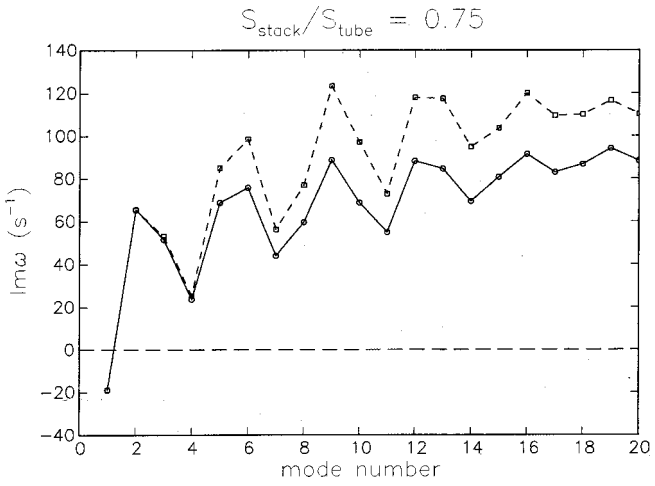

FIG. 6. Damping constant of the first 20 eigenmodes for the same case as in the previous figure, but including the 25% blockage (75% porosity) of finite-thickness plates.

mode is unstable. The results shown by the squares and the dashed line correspond to the differential equation formulation (20)–(22), while the triangles connected by the dotted line correspond to the simple formulation (13) and (14) for the exchange operators. Although both models give good results for the first few modes, the simple formulation (13)–(14) makes some higher modes negatively damped, i.e., unstable; this circumstance was at the root of the numerical difficulties encountered in our previous work (Yuan *et al.*, 1997). On the other hand, the differential equation approximation (20)–(22) gives a good agreement with the linear-theory results for the first few modes and reasonable estimates for the higher modes. Since the fraction of energy contained in these higher modes is usually very small, the associated error is likely to be acceptable.

These numerical results are for a system consisting of a 1-m-long cylindrical tube filled with helium ($\gamma=5/3$, $\sigma=0.71$, $c_p=5.2$ kJ/kg K). The stack has a length of 30 mm and consists of parallel plates of negligible thickness spaced by 0.77 mm. The radius of the tube is assumed to be large so that drag and heat transfer effects are small outside the stack region. The mean pressure is 307 kPa. The tube wall temperature at the left of the stack is $T_C=293$ K, and at the right $T_H=415$ K, so that $T_H-T_C=122$ K. In the stack region the wall temperature is independent of time and a linear function of position. Over the temperature range of interest the thermal conductivity data were fitted by a linear function of temperature as $k=0.151+3.228\times10^{-4}(T-300)$, with k in W/m K and T in K. We have included this effect in the calculations as the value of k determines the thermal penetration thickness, and therefore has a significant impact on the heat transfer parameters. The frequencies ω_1 and ω_2 were evaluated using the approximation (30).

The present model can accommodate tubes with a non-uniform cross section. To illustrate this effect, we show in Fig. 6 results similar to Figs. 3–5 but including the blockage caused by a finite stack-plate thickness. Here, $S_{\text{stack}}/S_{\text{tube}}=0.75$ and the stack is positioned at $x_s/L=0.684$. As another example, in Figs. 7 and 8 we consider a tube with a cross-sectional area given by

$$\frac{S(x)}{S(0)}=\begin{cases}1 & 0\leqslant\frac{2}{5}L\\ [1+Z\,\cos^2\{5\pi/2(2x/L-1)\}]^2 & \frac{2}{5}L\leqslant x\leqslant\frac{3}{5}L,\\ 1 & \frac{3}{5}L\leqslant x\leqslant L\end{cases}\tag{31}$$

for Z equal to 0.4 and -0.4, respectively; the stack position is $x_s/L=0.684$ and the thickness of the stack plates is neglected. In all these examples the frequencies ω_1 and ω_2 were evaluated using the simple approximation (30), which remains fairly accurate in spite of the cross section variation. For example, for the case of (31) with $Z=0.4$, the error for the fundamental mode is less than 3% and for the second mode about 10%.

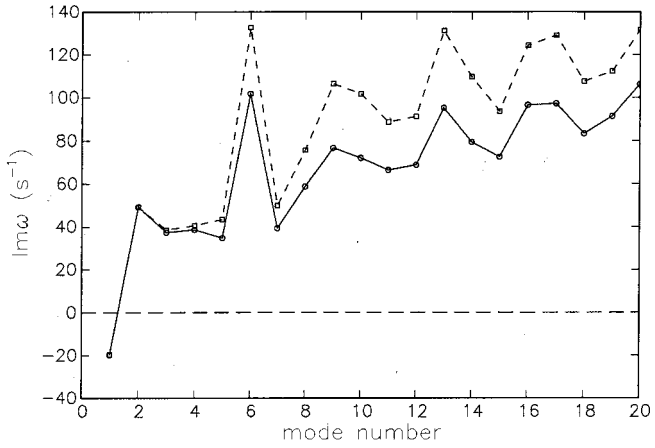

FIG. 7. Damping constant of the first 20 eigenmodes for a resonator with a wider midsection according to (31) with $Z=0.4$; see Sec. IV for a description of the system modeled. The stack is located at $x_s/L=0.684$ as in the previous two figures. The circles are the results of Rott's linear theory. The squares and triangles correspond to the differential equation approximation (20)–(22) to the momentum and energy exchange terms and to the simple explicit form (19), respectively. The lines are only meant as guides to the eye.

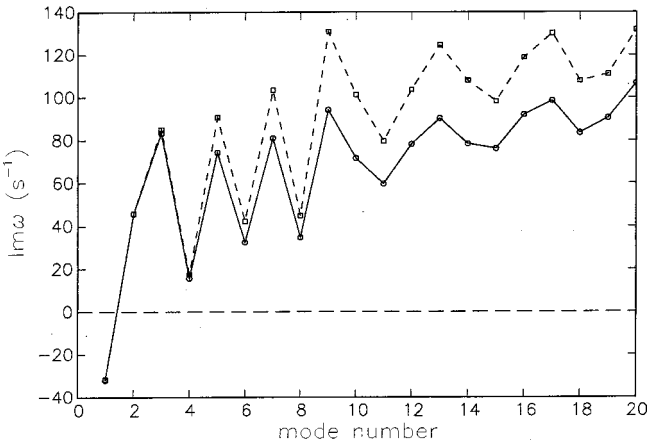

FIG. 8. As in the preceding figure, but with $Z=-0.4$.

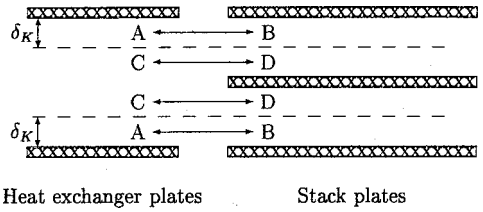

FIG. 9. Schematic representation of a case in which the gap between stack plates is half that between heat exchanger plates. The gas particles moving between points A and B exchange heat with the heat exchanger plates since the point A is within a thermal penetration depth δ_K. In contrast, the gas particles moving between points C and D do not exchange heat with the heat exchanger plates. Therefore, the middle stack plate does not participate in the heat transport along the stack.

V. NUMERICS

In order to solve the equations of the present model numerically, we use the total-variation-diminishing scheme of Harten (1983) described in Yuan *et al.* (1997), to which the reader is referred for details. This method has proven to be effective, robust, and accurate. It is second-order accurate in space, except near regions of very rapid variation of the solution, where it prevents the appearance of the spurious oscillations which contaminate the more traditional schemes.

Since, as is well known (see, e.g., Cao *et al.*, 1996), sharp temperature gradients exist near the ends of the stack while the fields are smooth away from the stack region, the use of a variable spatial node spacing improves efficiency. For the numerical examples that follow, in which the tube length is approximately 1 m, a node spacing Δx of 1 mm outside the stack region and 0.25 mm inside the stack gave converged results.

The time integration is explicit, with the time step Δt chosen on the basis of a CFL criterion $\max(c\Delta t/\Delta x \leqslant)$ 0.4, where Δx is the length of the spatial step and c the local speed of sound; the maximum is evaluated over the entire grid at each time step. With the estimate (30) of the time scale of the oscillations, this choice gives $\omega_1 \Delta t \simeq 0.2\ \Delta x/L$ and is therefore adequate to accurately track the time evolution of the system.

VI. ILLUSTRATIVE RESULTS

In order to illustrate the behavior of the model described before, we now consider several examples: a prime mover with a temperature gradient above onset, an externally driven thermoacoustic refrigerator, and a prime mover/refrigerator combination.

A. Prime mover

The first example is a model of the prime mover system studied by Atchley *et al.* (1990b) and Atchley (1992, 1994). It consists of a 38.2-mm-diameter tube with a length of 99.89 cm, a stack of 35 stainless-steel plates located 90.13 cm from the cold end, and two heat exchangers. The plates are 35 mm long, with a thickness of 0.28 mm and a spacing of 0.77 mm. We take handbook values for the physical properties: $\rho_s = 7900$ kg/m^3, $c_s = 480$ J/(kg K), $k_s = 14.9$ W/(m K). The cold heat exchanger at the left end of the stack consists of two identical structures separated by 1.5 mm, each with 25 nickel plates 0.45 mm thick, spaced by 1.04 mm and 10.2 mm. The hot heat exchanger is attached to the right of the stack and is built like the cold one except that it consists of only one 7.62-mm-long structure. The area blockage is about 30% (70% porosity) in the heat exchangers and 27% (73% porosity) in the stack.

In this system, a feature to be noted is the difference in the number of stack and heat exchanger plates. For the conditions of the experiment the thermal penetration length at the temperature of the cold heat exchanger is approximately 0.19 mm, which is about 25% of the stack plate spacing but only 18% of the heat exchanger plate spacing. At the hot heat exchanger temperature, $\delta_K \simeq 0.38$ mm and the corresponding ratios are 49% and 37%. Since a gas particle only exchanges heat if it is within 1–2 thermal penetration lengths from the plates, as sketched in Fig. 9, it may be expected that some of the stack plates are effectively not contributing as the gas particles that move along them make only an imperfect thermal contact with the heat exchangers, particularly at the cold end where δ_K is smaller.

To account in a rough way for this effect, one may say that only as many stack plates as there are heat exchanger plates take part in the heat transfer. Alternatively, the effect of each stack flow passage, as represented by the heat exchange terms $\mathcal{H}$ and $\mathcal{Q}$, should be reduced by a factor $K_h = 25/35 \simeq 0.71$.

In order to show that this is a reasonable estimate we first consider the linear case. With the correction factor K_h, upon linearization and in the frequency domain, in place of (11) the system (1) to (3) leads to the following eigenvalue equation for the pressure perturbation p':

$$\frac{1}{S}\frac{d}{dx}\left[\frac{Sc_A^2}{1+\hat{D}(\omega)/(i\omega)}\frac{dp'}{dx}\right]+K_h\frac{\hat{H}(\omega)}{i\omega}\frac{c_A^2}{S}\frac{d}{dx}$$
$$\times\left[\frac{S}{1+\hat{D}(\omega)/(i\omega)}\frac{dp'}{dx}\right]+\left(1+K_h\,\gamma\,\frac{\hat{H}(\omega)}{i\omega}\right)\omega^2 p'$$
$$+K_h\,\hat{Q}(\omega)\,\frac{(\gamma-1)c_p}{1+\hat{D}(\omega)/(i\omega)}\frac{dT_w}{dx}\frac{dp'}{dx}=0, \qquad (32)$$

where, as before, c_A is the local adiabatic sound speed and $\hat{D}(\omega)$, $\hat{H}(\omega)$, and $\hat{Q}(\omega)$ are defined in (13) and (14).

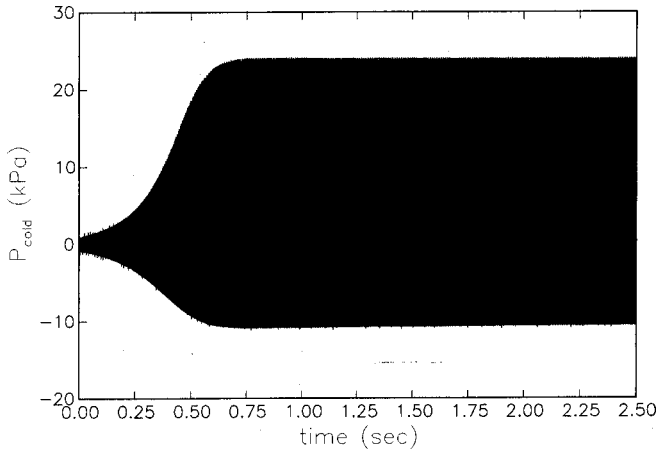

FIG. 10. Transient behavior of the pressure at the cold end of the tube for a prime mover with a temperature difference $T_H - T_C = 368$ K described by Atchley *et al.* (1990b).

In the experiments of Atchley *et al.* (1990b) the temperature difference of 325 K was slightly above onset. A solution of Eq. (32) gives an onset temperature difference of 279.6 K for $K_h = 1$ and 319.1 K for $K_h = 0.71$. From the data reported in Atchley (1994), for a mean pressure of 376 kPa and a temperature difference along the stack of 379 K, the linear temporal growth rate of the perturbation is 5.0 s^{-1}. The solution of Eq. (32) gives a linear growth rate of 11.87 s^{-1} for $K_h = 1$ and 5.64 for $K_h = 0.71$. Obviously, the correction embodied in K_h gives a much better agreement of the linear theory with the experimental results and, for this reason, we feel justified in using the same correction factor K_h for the nonlinear problem as well.

Figures 10 and 11 show the transient and steady-state temporal waveforms of the pressure at the cold end of the tube for the case with a temperature difference $T_H - T_C = 368$ K described by Atchley *et al.* (1990b). The calculation is started with a linear temperature distribution in the stack and a small amplitude of the first system normal mode. The helium mean pressure is 307 kPa. Figure 12 shows the temperature deviation from the initial value as a function of time

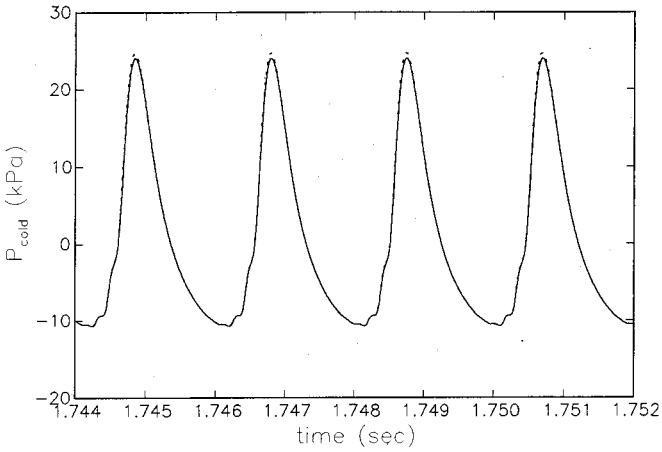

FIG. 11. Steady-state temporal waveform of the pressure at the cold end of the tube for the prime mover of the previous figure. The dotted line corresponds to a fixed linear temperature distribution in the stack; the solid line is calculated with the numerically determined steady-state temperature distribution at the end of the transient.

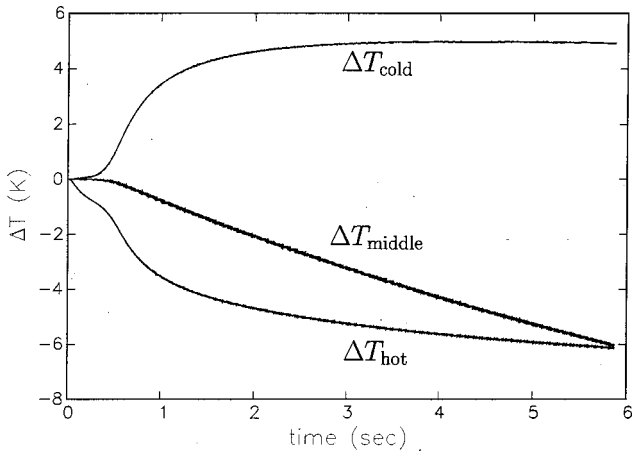

FIG. 12. Temperature deviation from the initial value as a function of time at the center of the stack and 1 mm away from the cold and hot ends for the prime mover of the previous two figures. Initially the temperature near the cold end increases and that near the hot end decreases very rapidly. The difference between the initial and steady-state temperature is approximately 5 and 6 K for the cold and hot ends of the stack, respectively. In contrast, the temperature in the middle of the stack decreases slowly to its steady-state value (not shown in this figure). The final stack temperature distribution is shown in the next figure.

at the center of the stack and 1 mm away from its cold and hot ends. The temperature near the cold end increases and that near the hot end decreases rapidly during the first second, after which they slowly reach the steady-state values. The difference between the initial and steady-state temperatures is approximately 5 and 6 K for the cold and hot ends of the stack, respectively. In contrast, the temperature in the middle of the stack decreases slowly to its steady-state value (not yet achieved in this figure). The final stack temperature distribution averaged over one cycle is shown in Fig. 13. The solid line is the mean wall temperature and the dotted line the mean gas temperature. One can see that there are near-jumps in the temperature of the solid structure at the ends of the stack. The correctness (at least qualitative) of this result is confirmed by the experiments and analysis of Brewster *et al.* (1997) and the calculations of Worlikar (1997) and Worlikar *et al.* (1998). These near-jumps effectively reduce

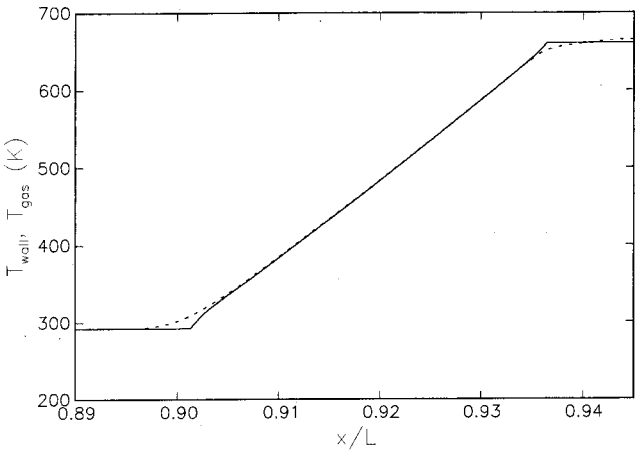

FIG. 13. The final mean temperature distribution in the stack (solid line) and in the gas (dotted line) for the prime mover of the previous three figures. Note the jumps in the solid structure temperature at the ends of the stack.

the available temperature difference in the stack, thus reducing the steady-state oscillation amplitude in comparison with what would be obtained by assuming a time-independent linear stack temperature distribution equal to $T_H - T_C$. This effect is shown in Fig. 11 by the dotted line, which represents the results with the assumption that the wall temperature in the stack region is a time-independent linear function of position. For this particular case the difference between the two results is however small. Figure 11 should be compared with Fig. 4 of Atchley *et al.* (1990b). Qualitatively, the numerical results are close to the experimental ones. The period, 1.95 ms, is identical within the precision with which it can be read from the figure. The waveform exhibits a strong asymmetry, with the negative amplitude much smaller than the positive one. The major difference between calculations and experiment is the amplitude, which is about 24.0 kPa in Fig. 11, but 13.5 kPa in the data. In order to match with measured wave amplitude, the temperature difference $T_H - T_C$ should be decreased by about 25 K. A possible explanation for this difference may be the following. First, the temperature values reported in Atchley *et al.* were measured at the surface of the tube, rather than in the middle of the heat exchanger plates. For the conditions of the experiment it is not unreasonable to expect a temperature difference of the order of 10–20 K between these two points.[6] In addition, the experimental setup most likely includes several loss mechanisms (e.g., form drag of the plates, natural convection) not included in our model.

B. Piston-driven refrigerator

Now, we consider a simple model of a thermoacoustic refrigerator in which a piston at the left end of the tube sets up a standing wave; the right end is modeled as rigid.

The driving frequency is equal to the natural frequency of the tube open at one end, namely $\omega = 2\pi\sqrt{\gamma \mathcal{R} T_i}/(4L)$, where $L = 0.5$ m is the tube length and $T_i = 293$ K the initial uniform temperature of the gas and solid structures. An oscillating velocity $u(t) = U_A \sin \omega t$ is prescribed at $x = 0$ and $p' = \rho' = T' = 0$ there as discussed at the end of Sec. II. The gas is helium at a mean pressure $P_0 = 307$ kPa. The stack consists of 0.28-mm-thick, 30-mm-long plates spaced by 0.77 mm with a thermal conductivity of $k_s = 0.48$ W/(K m) characteristic of fiberglass. It is well known from linear theory (see, e.g., Swift, 1988; Karpov and Prosperetti, 1998) that the thermoacoustic heat flux is strongest when the stack is positioned midway between a velocity node and antinode. Since in this case the tube length is one-quarter of the acoustic wavelength, we position the stack at $x_s/L = 0.5$.

The hot heat exchanger is modeled by assuming a spatially and temporally constant temperature. The cold heat exchanger is assumed to be unloaded and to only exchange heat with the gas and the stack. It is therefore modeled assuming a spatially uniform, time-dependent temperature, the mean value of which will decrease with time under the action of the sound waves. Since the thermal conductivity is assumed to be very large, this cold heat exchanger is simply characterized by the product $\rho_s c_s$. The duration of the transient of the system increases with the value of this quantity and therefore, in order to limit the computational time, we choose $\rho_s c_s = 480$ kW/(K m^3) which is about one order of magnitude smaller than the appropriate value for realistic materials. In spite of this limitation, the results that follow are useful to demonstrate the performance of the model. For simplicity, we disregard blockage effects and take both f_V and f_K to vanish outside the stack and heat exchanger region, thus neglecting momentum and energy exchange with the resonator tube walls.

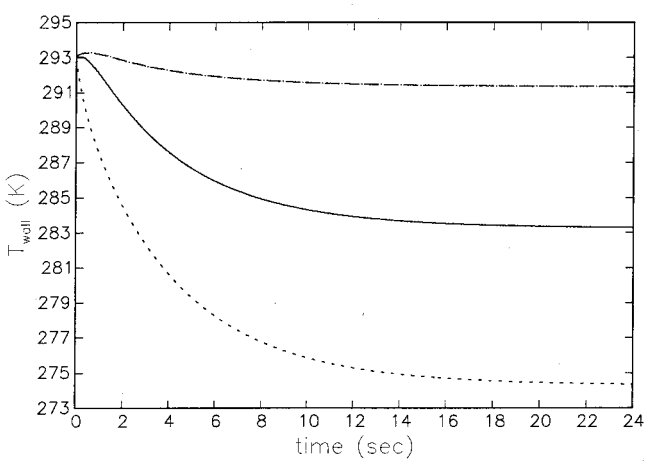

FIG. 14. Mean wall temperature as a function of time at the cold heat exchanger (dotted line), at the stack midpoint (solid line), and 1 mm away from the hot heat exchanger (dot-dash line) for a driven tube with a drive ratio of 4%. The final temperature difference between the heat exchangers is 18.5 K.

Figure 14 shows the temperature T_w as a function of time at the cold heat exchanger (lowest line), at the stack midpoint (middle line), and 1 mm away from the end of the hot heat exchanger. Here, the imposed velocity amplitude U_A is 24.2 m/s which, when converted to pressure according to the standard acoustic relation $U_A = P_A/\rho c_A$, corresponds to a drive ratio $P_A/P_0 = 0.04$. The temperature of the cold heat exchanger initially decreases with time and finally stabilizes at about 18.5 K less than the initial temperature. At steady state, on average, the heat extracted from the heat exchanger by the gas must balance the heat gained by conduction from the stack plates. Thus, the acoustic power supplied to the

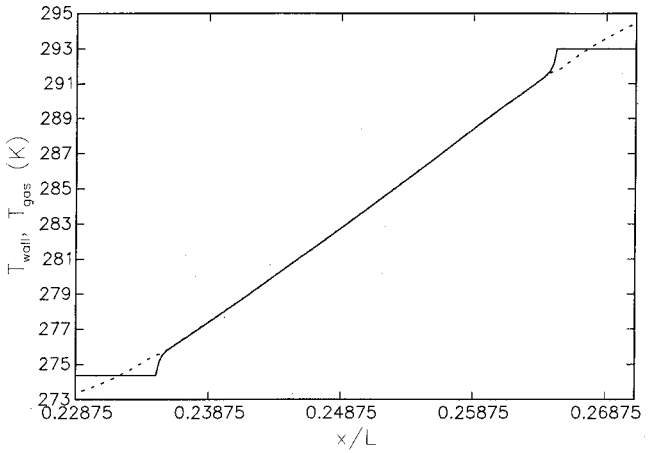

FIG. 15. Mean steady-state temperature distribution in the region of the stack and the heat exchangers for the solid surfaces (solid line) and the gas (dotted line) for the driven tube of the previous figure.

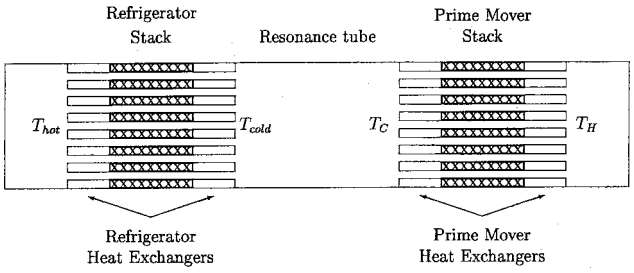

FIG. 16. Schematic representation of a thermoacoustic prime mover/thermoacoustic refrigerator combination. A temperature difference $T_H - T_C$ is maintained across the prime mover stack by its heat exchangers. The standing wave generated by the prime mover stack causes a temperature difference across the refrigerator stack.

system by the piston is spent only to maintain this steady state by removing during each cycle the same amount of heat from the cold heat exchanger that it receives from the stack by conduction. Figure 15 shows the final mean temperature distribution in the region of the stack and the heat exchangers. The mean temperature of the solids is shown by the solid line, and that of the gas by the dotted line. There are near-jumps in the temperature of the solid structure at the ends of the stack similar to those found in Fig. 13. Note that a significant difference between the gas and solid structure temperatures occurs only in the heat exchanger regions, whereas the temperature of the gas and the plates is almost the same over most of the stack. The mean temperature of the gas is higher than that of the solid structure over one part of the heat exchanger, and lower over the other part. The same result was found in the two-dimensional calculation of Worlikar (1997), Worlikar and Knio (1999), and Mozurkewich (1998b).

C. Thermoacoustic refrigerator coupled with prime mover

As a final example, we consider the combination of a thermoacoustic prime mover and a thermoacoustic refrigerator sketched in Fig. 16 housed in a 1-m-long rigidly terminated tube. The prime mover stack is located in the right part

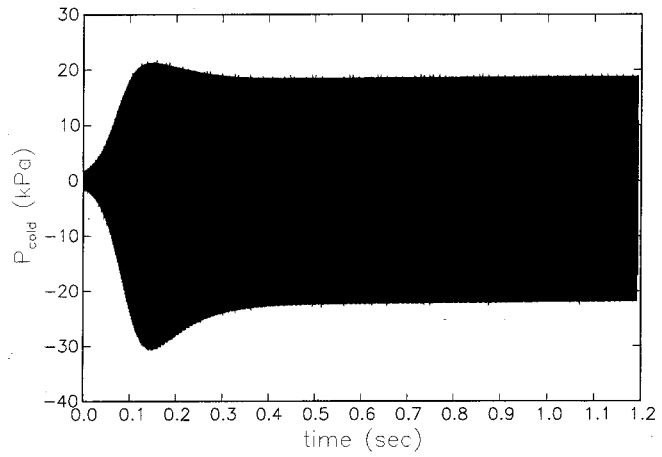

FIG. 17. Transient behavior of the pressure at the cold end of the tube for the thermoacoustic prime mover/refrigerator combination sketched in the previous figure. Note the nonmonotonic behavior of the pressure amplitude.

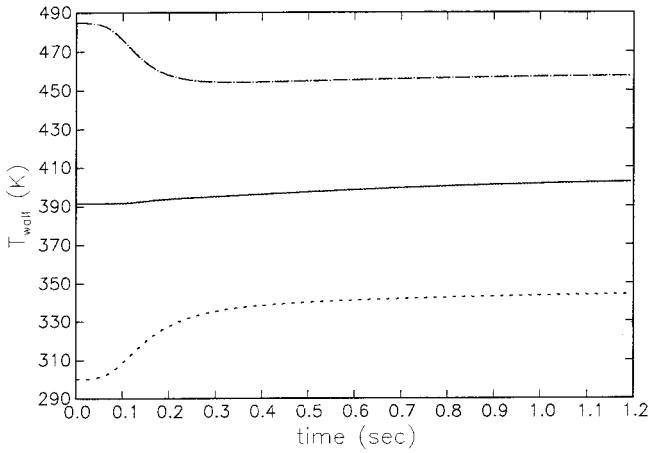

FIG. 18. Temperature vs time at three positions in the prime mover stack for the thermoacoustic prime mover/refrigerator combination of the previous two figures. The dot-dash and dotted lines are for points 1 mm away from the hot and cold heat exchangers, respectively; the solid line is for the stack midpoint. The initial temperature gradient of 6.67 K/mm is reduced to only 4 K/mm at steady state.

of the tube at $x_s/L = 0.26$ and the standing wave that it generates induces a temperature difference across the refrigerator stack positioned in the left part of the tube at $x_s/L = 0.73$.

As before, we neglect blockage effects and gas–solid momentum and energy exchanges away from the stack/heat exchangers region. The gas is helium at a mean pressure of 307 kPa. The stacks and heat exchangers consist of 0.28-mm-thick parallel plates spaced by 0.77 mm with a length of 30 and 1.5 mm, respectively. For the same reasons mentioned above we set the product $\rho_s c_s$ to 480 kW/(K m^3). The thermal conductivity of the stack plates is $k_s = 0.48$ W/(K m) as before, whereas the plates of the refrigerator heat exchangers are assumed to have infinite thermal conductivity. The temperature of the prime-mover heat exchangers is prescribed to be $T_C = 293$ K, $T_H = 493$ K, and held fixed. The temperatures of the refrigerator heat exchangers are allowed to change in a manner similar to the cold heat exchanger of the previous example. Initially the temperature is a uniform

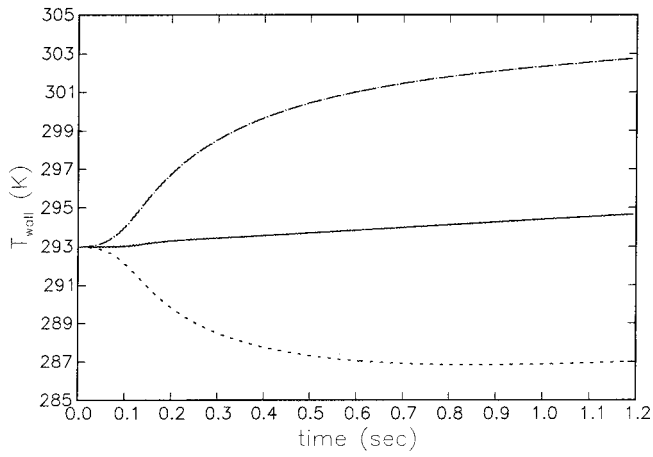

FIG. 19. Temperature vs time of the cold (dotted line) and hot (dot-dash line) heat exchangers and the stack midpoint (solid line) in the refrigerator unit of the thermoacoustic prime mover/refrigerator combination of the previous three figures.

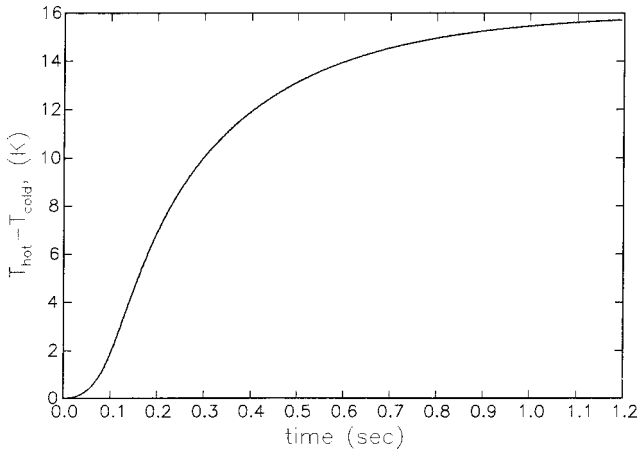

FIG. 20. Temperature difference between the two heat exchangers versus time in the refrigerator unit of the thermoacoustic prime mover/refrigerator combination of the previous figures.

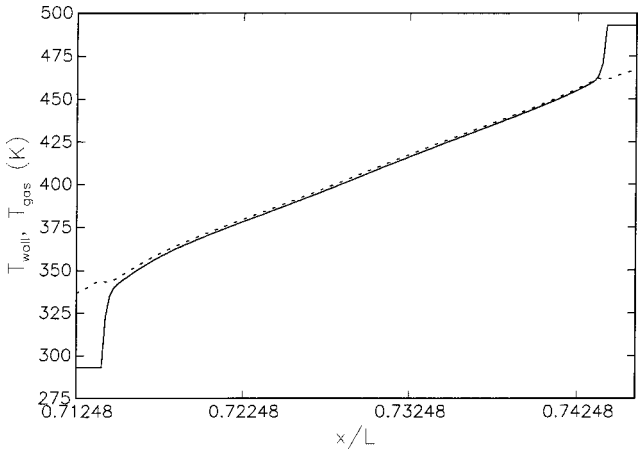

FIG. 22. Mean steady-state temperature distributions in the prime-mover stack and connected heat exchangers for the solid surfaces (solid line) and the gas (dotted line) for the thermoacoustic prime mover/refrigerator combination sketched in Fig. 16.

293 K along the refrigerator stack, while it is a linear function along the prime mover stack.

Figure 17 shows the pressure at the cold end of the tube as a function of time. There is an initial fairly rapid rise up to a maximum amplitude reached at about 0.15 s, followed by a decline to the steady-state regime which is essentially attained at 0.4 s. In order to understand this nonmonotonic behavior, we show in Fig. 18 the temperature at three positions in the prime-mover stack, the midpoint, and 1 mm away from each end. We see here that the temperatures near the two ends of the stack move in opposite directions, approaching each other so much so that the initial temperature gradient of 6.67 K/mm prevailing along most of the stack is reduced at steady state to only 4 K/mm (except for the 1-mm-long segments adjacent to the heat exchangers). The amplitude decrease of Fig. 17 clearly occurs as a consequence of this trend. While the pressure reaches steady state at about 0.4 s, the stack temperatures continue to slowly adjust after this time but without a significant change in the temperature gradient.

Turning now to the refrigerator section, we show in Fig. 19 the temperatures of the two heat exchangers and of the stack midpoint, all as functions of time. The temperatures of the cold and hot heat exchangers initially move in opposite directions, as expected. However, after about 1.0 s, the temperature of the cold heat exchanger starts increasing due to viscous and thermal heating of the refrigerator stack and its heat exchangers. For the refrigerator stack the temperature changes much more slowly than for the prime-mover stack, reaching its steady state only after 1.2 s. Figure 20 shows the temperature difference between the two refrigerator section heat exchangers as a function of time.

Figures 21 and 22 show the final mean temperature distributions for the refrigerator and prime-mover stacks and connected heat exchangers. Significant temperature differences between the plates (solid lines) and the gas occur only near the heat exchangers. For the refrigerator stack the gas temperature is higher than the solid temperature over one part of the heat exchanger and lower over another part, as found before.

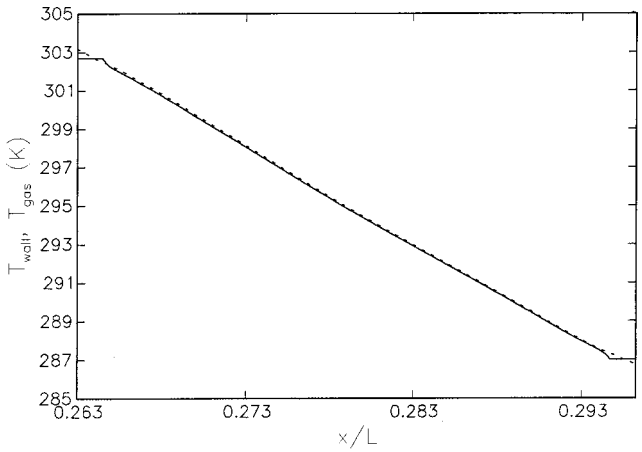

FIG. 21. Mean steady-state temperature distributions in the refrigerator stack and connected heat exchangers for the solid surfaces (solid line) and the gas (dotted line) for the thermoacoustic prime mover/refrigerator combination sketched in Fig. 16.

VII. CONCLUSIONS

The mathematical model of thermoacoustic prime movers and heat pumps presented in this paper derives from an earlier formulation by the authors (Watanabe *et al.*, 1997; Yuan *et al.*, 1997). With respect to that model the present one has been considerably improved in a key respect, namely the modeling of momentum and energy exchanges between the gas and the solid boundaries with which it is in contact. The present model is more realistic (as it well approximates the linear results of Rott's theory for a significant number of modes) and, as an added advantage, is more numerically robust. The previous formulation has been improved in another significant respect, in that the temperature of the solid surfaces of the device is now calculated rather than prescribed.

The model described in this paper is quite flexible as demonstrated by the examples that we have presented: a prime mover, a combined prime mover/refrigerator system, and a piston-driven refrigerator. We have been able to follow in the time domain the evolution of these systems and, for

the first two, we have presented results that trace the evolution of the initial linear instability to the nonlinear regime, and finally to steady state where the instability saturates to a finite amplitude. This is a specifically nonlinear effect that cannot possibly be captured by models based on a linear approximation. We have also tested the model successfully for the prime mover/refrigerator combination assuming periodicity boundary conditions; we have not shown these results as, for the conditions tested, the system turned out to be stable.

It is apparent from the formulation presented in Secs. I, III, and IV, that the model includes several nonlinear mechanisms. In the first place, it accounts for mode–mode coupling. Even though in actual thermoacoustic engines the resonator is built so as to detune the harmonics, at sufficiently large amplitudes a coupling still exists and represents a significant mechanism for energy loss. In a thermoacoustic engine, typically it is only the fundamental mode that is unstable, while all higher modes are damped. Hence, energy leaking out of the fundamental mode into higher ones is dissipated; a weakly nonlinear analysis of this phenomenon is presented in Karpov and Prosperetti (2000). Similarly, in a refrigerator the stack is badly positioned with respect to the spatial distribution of pressure and velocity for modes other than the fundamental, which leads to a loss of efficiency. Secondly, the model does not contain any limitation on the displacement s of the fluid particles and, therefore, it dispenses with the standard assumption of linear theory in which $s\, dT_w/dx \ll T_w$. Third, although the models for the cross-stream momentum and heat exchange are patterned after the linear form (justified by the fact that, typically, the stack is many hydraulic diameters long), we do retain the dependence on the local temperature and pressure thus recovering, at least in part, the mechanism of thermal harmonic wave generation described in Gusev *et al.* (2001).

Some streaming effects [and, in particular, the pressure buildup in the direction of the tube ends, see Waxler (2001)] are included due to the nonlinearities retained in the cross-sectional averaged model, but others (specifically the Rayleigh streaming due to boundary layer effects) are not. In any event, the role of streaming in thermoacoustic systems does not seem to have been completely elucidated (see, e.g., Olson and Swift, 1998; Gopinath *et al.*, 1998; Gusev *et al.*, 2000; Bailliet *et al.*, 2001; Waxler, 2001).

Absent from the model are transition/turbulence phenomena in the stack and vortex shedding from geometric discontinuities such as the ends of the stack and of the heat exchangers. While the impact of the latter on momentum transfer could possibly be accounted for by lumped resistances in a finite-difference implementation, inclusion of the former would require a modification of the exchange parameters $\mathcal{D}$, $\mathcal{H}$, and $\mathcal{Q}$. Two-dimensional nonlinear simulations suggest the presence of some transitional effects only at very high drive ratios, in excess of 6% (Besnoin, 2001). As for the impact of vortex shedding on heat transfer, their significance and role is still an open question.

While these and other mechanisms and other details of a real thermoacoustic system may not be easily incorporated in the present model, a great variety of design parameters can be accounted for such as geometry (and in particular a nonconstant cross section), physical properties, temperature conditions, standing and traveling waves, and others. Thus we believe that—at the very least—the present model can be used in a relative sense to compare the effect of proposed design modifications and to gain insight into the performance of new systems.

ACKNOWLEDGMENT

The authors express their gratitude to the Office of Naval Research for the support of this work.

APPENDIX: MODELING OF HEAT EXCHANGE

Heat transfer between the solid structure and the fluid in Eqs. (3) and (5) is modeled in a somewhat unconventional manner which warrants some clarification (see also Watanabe *et al.*, 1997).

Application of cross-sectional averaging to the exact energy balance equation for the fluid gives $(\mathcal{P}/S)\ \overline{\mathbf{q}\cdot\mathbf{n}}$, where $\mathcal{P}$ is the perimeter of the ''wetted'' area and $\overline{\mathbf{q}\cdot\mathbf{n}}$ is the area-averaged heat flux out of the gas. What we have done in Eq. (3) is to set

$$\frac{\mathcal{P}}{S}\,\overline{\mathbf{q}\cdot\mathbf{n}} = \rho c_p \left[\mathcal{H}(T_w - T) - \frac{dT_w}{dx}\mathcal{Q}\, u \right]. \tag{A1}$$

The parametrization that we use is motivated by the results of the linear theory for cross-stream energy exchange according to which, in the frequency domain (Watanabe *et al.*, 1997),

$$\frac{\mathcal{P}}{S}\,\overline{\mathbf{q}\cdot\mathbf{n}} = \rho c_p \frac{i\omega f_K}{1-f_K}(T_w - T) - \frac{1}{1-\sigma} \times \left(\frac{f_v}{1-f_v} - \frac{\sigma f_K}{1-f_K} \right) \rho c_p \frac{dT_w}{dx}\, u. \tag{A2}$$

Here, as before, T and u are the cross-section averaged fluid temperature and velocity. The coefficient of $T_w - T$ in the first term is just a generalization of the standard heat transfer coefficient. Indeed, if we consider the limit of steady flow, in which $\omega \to 0$, using the asymptotic approximation of f_K [Watanabe *et al.*, 1997, Eq. (60)]

$$f_K = 1 - \frac{i l^2}{2\delta_K^2} + O\left(\frac{l}{\eta}\right)^4, \tag{A3}$$

we find

$$\overline{\mathbf{q}\cdot\mathbf{n}} \simeq 8\frac{k}{l}(T_w - T), \tag{A4}$$

which coincides with the standard result for steady, fully developed flow in a channel (see, e.g., Incropera and DeWitt, 1996, p. 430). The complex, ω-dependent form that appears in (A2) accounts for the phase relation that is crucial in an oscillatory flow. The same parametrization of this term as for the momentum transfer coefficient is justified by the similar-

ity between the two transfer processes, which is also apparent by the similar functional form of the two terms [cf. Eqs. (13) and (14)].

Of greater interest is the second term in (A2) which does not arise in conventional heat transfer, in which wall temperature gradients are usually not accounted for explicitly. The physics behind this term may be better understood if it is noted that linearization of the energy equation (3), use of the equation of state (4), and of the continuity equation (1) permit us to write

$$\rho c_p\left[i\omega T' + (1+\mathcal{Q})\, u\frac{dT_w}{dx}\right] - i\omega p' = -\mathcal{H}T', \qquad \text{(A5)}$$

where $T' = T - T_w$, $p' = p - P_0$. This relation shows that $\mathcal{Q}$ represents a correction to the convective transport term, the origin of which lies in the nonuniformity of the velocity distribution over the channel. Consider the enthalpy convected by the fluid during a time dt across a cross section located at x: the particles very near the wall will carry an enthalpy close to $c_p T_w(x)$, because they will have moved very little due to the no-slip condition. However, particles further way from the wall will come from further upstream, where the temperature is significantly different from $T_w(x)$. Thus, the enthalpy convected by the average velocity u should not be $c_p T_w(x)$, but should be modified: the factor $1+\mathcal{Q}$ has precisely the role to effect this modification. This analysis is supported by the fact that, in the absence of viscosity ($\sigma = 0$) the velocity distribution is uniform and one finds indeed $\mathcal{Q} = 0$ because, then, all the fluid particles transport the same enthalpy.

[1]Heat flow limitations in the heat exchangers can also affect the saturation level quantitatively; the existence of the saturation phenomenon itself, however, is a nonlinear effect.

[2]It appears possible to modify this equation to account for possible heat flow limitations of the heat exchangers (e.g., by adding a term mimicking, by means of a heat transfer coefficient, the coupling with external thermal reservoirs), although we do not pursue this possibility here.

[3]In Yuan *et al.* (1997) this definition was extended to the nonlinear domain by replacing $\partial/\partial t$ by the convective, or material, derivative. In later work (Karpov and Prosperetti, 2000) it was shown, however, that the nonlinear terms thus introduced have a very minor effect. For this reason, and in view of the uncertainty in the proper nonlinear extension, they are neglected here.

[4]The reader is reminded that the temperature and pressure variation of the physical properties are included in the present model.

[5]It is seen from (14) that Q is a combination of D and H. However, the presence of the factor $i\omega$ in these two quantities shows that the physical effect accounted for by D and H is in phase with the particle displacement, rather than the velocity, as the effect of Q. For this reason, in the time domain, it is not desirable to derive the expression of $\mathcal{Q}$ from those of $\mathcal{D}$ and $\mathcal{H}$, but to proceed directly as in (14).

[6]Since Atchley *et al.* do not report measurements of heat fluxes, it is not possible to estimate the likely temperature drop between the central region of the heat exchanger plates and the tube surface.

Achard, J. L., and Lespinard, G. M. (**1981**). ''Structure of the transient wall-friction law in one-dimensional models of laminar pipe flows,'' J. Fluid Mech. **113**, 283–298.

Arnott, W. P., Bass, H. E., and Raspet, R. (**1991**). ''General formulation of thermoacoustics for stacks having arbitrarily shaped pore cross sections,'' J. Acoust. Soc. Am. **90**, 3228–3237.

Atchley, A. A. (**1992**). ''Standing wave analysis of a thermoacoustic prime mover below onset of self-oscillation,'' J. Acoust. Soc. Am. **92**, 2907–2914.

Atchley, A. A. (**1994**). ''Analysis of the initial build-up of oscillations in a thermoacoustic prime mover,'' J. Acoust. Soc. Am. **95**, 1661–1664.

Atchley, A. A., Hofler, T. J., Muzzerall, M. L., Kite, M. D., and Ao, C. (**1990a**). ''Acoustically generated temperature gradients in short plates,'' J. Acoust. Soc. Am. **88**, 251–263.

Atchley, A. A., Bass, H. E., and Hofler, T. J. (**1990b**). ''Development of nonlinear waves in a thermoacoustic prime mover,'' in *Frontiers in Nonlinear Acoustics*, edited by M. F. Hamilton and D. T. Blackstock (Elsevier, Amsterdam), pp. 603–608.

Bailliet, H., Gusev, V., Raspet, R., and Hiller, R. A. (**2001**). ''Acoustic streaming in closed thermoacoustic devices,'' J. Acoust. Soc. Am. **110**, 1808–1821.

Bauwens, L. (**1996**). ''Oscillating flow of a heat-conducting fluid in a narrow tube,'' J. Fluid Mech. **324**, 135–161.

Bauwens, L. (**1998**). ''Thermoacoustics: Transient regimes and singular temperature profiles,'' Phys. Fluids **10**, 807–818.

Besnoin, E. (**2001**). ''Numerical Study of Thermoacoustic Heat Exchangers,'' Doctoral dissertation, Department of Mechanical Engineering, The Johns Hopkins University.

Brewster, J. R., Raspet, R., and Bass, H. E. (**1997**). ''Temperature discontinuities between elements of thermoacoustic devices,'' J. Acoust. Soc. Am. **102**, 3355–3360.

Cao, N., Olson, J. R., Swift, G. W., and Chen, S. (**1996**). ''Energy flux density in a thermoacoustic couple,'' J. Acoust. Soc. Am. **99**, 3456–3464.

Gopinath, A., Tait, N. L., and Garrett, S. L. (**1998**). ''Thermoacoustic streaming in a resonant channel: The time-averaged temperature distribution,'' J. Acoust. Soc. Am. **103**, 1388–1405.

Gusev, V., Job, S., Bailliet, H., Lotton, P., and Bruneau, M. (**2000**). ''Acoustic streaming in annular thermo-acoustic prime movers,'' J. Acoust. Soc. Am. **108**, 934–945.

Gusev, V., Lotton, P., Bailliet, H., Job, S., and Bruneau, M. (**2001**). ''Thermal wave harmonics generation in the hydrodynamical heat transport in thermoacoustics,'' J. Acoust. Soc. Am. **109**, 84–90.

Hamilton, M. F., Ilinski, Y. A., and Zabolotskaya, F. A. (**2002**). ''Nonlinear two-dimensional model for thermoacoustic engines,'' J. Acoust. Soc. Am. **111**, 2076–2086.

Harten, A. (**1983**). ''High resolution schemes for hyperbolic conservation laws,'' J. Comput. Phys. **49**, 357–393.

Ilinskii, Y. A., Lipkens, B., Lucas, T. S., van Doren, T. W., and Zabolotskaya, E. A. (**1998**). ''Nonlinear standing waves in an acoustical resonator,'' J. Acoust. Soc. Am. **104**, 2664–2674.

Incropera, F. P., and DeWitt, D. P. (**1996**). *Fundamentals of Heat and Mass Transfer*, 4th ed. (Wiley, New York).

Karpov, S., and Prosperetti, A. (**1998**). ''Linear thermoacoustic instability in the time domain,'' J. Acoust. Soc. Am. **103**, 3309–3317.

Karpov, S., and Prosperetti, A. (**2000**). ''Nonlinear saturation of the thermoacoustic instability,'' J. Acoust. Soc. Am. **107**, 3130–3147.

Mozurkewich, G. (**1998a**). ''A model for transverse heat transfer in thermoacoustics,'' J. Acoust. Soc. Am. **103**, 3318–3326.

Mozurkewich, G. (**1998b**). ''Time-average temperature distribution in a thermoacoustic stack,'' J. Acoust. Soc. Am. **103**, 380–388; **105**, 567(E) (1999). Erratum: ''Time-average temperature distribution in a thermoacoustic stack [J. Acoust. Soc. Am. **103**, 380–388 (1998)].

Olson, J. R., and Swift, G. W. (**1998**). ''Acoustic streaming in pulse tube refrigerator: Tapered pulse tubes,'' Cryogenics **37**, 769–776.

Rott, N. (**1969**). ''Damped and thermally driven acoustic oscillations in wide and narrow tubes,'' Z. Angew. Math. Phys. **20**, 230–243.

Rott, N. (**1976**). ''Thermally driven acoustic oscillations, IV: Tubes with variable cross section,'' Z. Angew. Math. Phys. **27**, 197–224.

Rott, N. (**1980**). ''Thermoacoustics,'' Adv. Appl. Mech. **20**, 135–175.

Strutt, J. W. (Lord Rayleigh) (**1896**). *The Theory of Sound* (Macmillan, London; reprinted by Dover, New York, 1945), Chap. 12.

Swift, G. W. (**1988**). ''Thermoacoustic engines,'' J. Acoust. Soc. Am. **84**, 1145–1180.

Watanabe, M., Prosperetti, A., and Yuan, H. (**1997**). ''A simplified model for linear and nonlinear processes in thermoacoustic prime movers. I. Model and linear theory,'' J. Acoust. Soc. Am. **102**, 3484–3496.

Waxler, R. (**2001**). ''Stationary velocity and pressure gradients in a thermoacoustic stack,'' J. Acoust. Soc. Am. **109**, 2739–2750.

Wheatley, J. (**1986**). ''Intrinsically irreversible or natural heat engines,'' in *Frontiers in Physical Acoustics*, edited by D. Sette (North-Holland, Amsterdam), pp. 35–475.

Worlikar, A. S. (**1997**). ''Numerical Simulation of a Thermoacoustic Refrigerator,'' Ph.D. dissertation, Johns Hopkins University.

Worlikar, A. S., and Knio, O. M. (**1996**). ''Numerical simulation of a thermoacoustic refrigerator. I: Unsteady adiabatic flow around the stack,'' J. Comput. Phys. **127**, 424–451.
Worlikar, A. S., and Knio, O. M. (**1999**). ''Numerical study of oscillatory flow and heat transfer in a loaded thermoacoustic stack,'' Numer. Heat Transfer **35**, 49–65.
Worlikar, A. S., Knio, O. M., and Klein, R. (**1998**). ''Numerical simulation of a thermoacoustic refrigerator. II Stratified flow around the stack,'' J. Comput. Phys. **144**, 299–324.
Yuan, H., Karpov, S., and Prosperetti, A. (**1997**). ''A simplified model for linear and nonlinear processes in thermoacoustic prime movers. II. Nonlinear oscillations,'' J. Acoust. Soc. Am. **102**, 3497–3506.